*Chapter 4*

AEOLIAN PROCESSES IN PROCTOR CRATER ON MARS: 2.
MESOSCALE MODELING OF DUNE-FORMING WINDS

Lori K. Fenton and Mark I. Richardson

Division of Geological and Planetary Sciences, California Institute of Technology, Pasadena, California

Anthony D. Toigo

Center for Radiophysics and Space Research, Cornell University, Ithaca, New York

**Abstract.** Both atmospheric modeling and spacecraft imagery of Mars are now of sufficient quality that the two can be used in conjunction to acquire an understanding of regional- and local-scale aeolian processes on Mars. We apply a mesoscale atmospheric model adapted for use on Mars to Proctor Crater, a 150 km diameter crater in the southern highlands. Proctor Crater contains numerous aeolian features that indicate wind direction, including a large dark dunefield with reversing transverse and star dunes containing three different slipface orientations, small and older bright duneforms that are most likely transverse granule ripples, and seasonally erased dust devil tracks. Results from model runs spanning an entire year with a horizontal grid spacing of 10 km predict winds aligned with two of the three dune slipfaces as well as spring and summer winds matching the dust devil track orientations. The primary (most prevalent) dune slipface direction corresponds to a fall and winter westerly wind created by geostrophic forces. The tertiary dune slipface direction is caused by spring and summer evening katabatic flows down the eastern rim of the crater, influencing only the eastern portion of the crater floor. The dunes are trapped in

the crater because the tertiary winds, enhanced by topography, counter transport from the oppositely oriented primary winds, which originally carried sand into the crater. The dust devil tracks are caused by light spring and summer westerly winds during the early afternoon caused by planetary rotation. The secondary dune slipface direction is not predicted by model results from either the Mars MM5 or the GFDL Mars GCM. The reason for this is not clear, and the wind circulation pattern that creates this dune slipface is not well constrained. The Mars MM5 model runs do not predict stresses above the saltation threshold for dune sand of the appropriate size and composition. As with previous work, the calculated wind velocities are too low, which may be caused by too large a grid spacing.

## 1. Introduction

The dominance of wind action over other contemporary surface processes on Mars became evident during the Mariner 9 mission in 1971–1972 [*e.g., McCauley et al.,* 1972; *Sagan et al.,* 1972; *Smith,* 1972; *Cutts and Smith*, 1973; *Arvidson,* 1974]. Wind circulation patterns determine the location and magnitude of sources, sinks, and transport pathways of particulate materials. Because of this coupling between surface materials and the atmosphere, the study of one is not complete without the study of the other. In particular, dune morphology is dependent on winds that are strong enough to saltate sand. Thus a study of dune morphology leads to an understanding of the orientations of strong local winds. Furthermore, there are few wind measurements available for use as "ground truth" of atmospheric models. Aeolian features are often aligned with the winds that formed them, providing the only indicator of surface wind direction than spans the globe. Thus a comparison of modeled wind predictions with orientations of surface features is the only current verification technique for both the modeled surface winds and

the applied boundary layer scheme. It is the atmospheric counterpart to surficial geology that is discussed in this work.

Shortly after the discovery of sand dunes on Mars, experimental work in wind tunnels began in order to better understand the physics behind sand saltation under Martian atmospheric conditions [*Iversen et al.*, 1973; *Iversen et al.*, 1976]. The results indicate that there are many differences in the mechanics of saltation on Mars and Earth. *Greeley et al.* [1980] found that threshold friction speeds an order of magnitude larger than those measured on the Earth are required to move similarly sized sand grains on Mars ($u_{*t}$ of 0.22 m s$^{-1}$ for Earth versus 2.2 m s$^{-1}$ for Mars). *Iversen and White* [1982] improved on previous work, producing new empirical relations for threshold friction speeds. They found that saltating particles on Mars would have longer path lengths than those on Earth, and that this parameter varies with temperature and atmospheric conditions. In addition, *White* [1979] showed that although it takes stronger winds to saltate sand on Mars, once saltation begins, the sand flux on Mars would be significantly higher than that on Earth. Now that sand grain sizes and compositions are being constrained using Thermal Emission Spectrometer (TES) data from the Mars Global Surveyor (MGS), a more precise estimate of saltation threshold stresses may be utilized in detecting sand saltation and calculating sand mass fluxes.

In the last decade, atmospheric models have been applied in conjunction with the results from wind tunnel experiments to better understand aeolian processes on Mars. *Greeley et al.* [1993] used a Mars general circulation model (GCM) to study the correlation of surface wind patterns to aeolian features with measurable wind orientations. They found that bright depositional streaks correspond well to the southern summer Hadley circulation, but that dark erosional streaks and yardangs did not agree well with any modeled winds above the saltation threshold. *Fenton and Richardson* [2001b] later found that a higher time resolution (hours rather than

days) in a Mars GCM resolved the nighttime winds that correlated well with dark erosional streaks, implying that temporal and spatial resolution in models is one of the keys to understanding some of the previously unexplained aeolian features. Yardang orientations remain unaligned with current winds, but some of these features may be so old that they were formed under ancient and unconstrained wind conditions that cannot be properly modeled without further information. Other applications of modeling the Martian surface on a regional or global scale have included finding bimodal winds in an area where longitudinal dunes indicate such a wind regime should exist [*Lee and Thomas*, 1995]; locating global sand sources and sinks [*Anderson et al.*, 1999]; and looking for changes in surface wind patterns caused by variations in orbital parameters [*Fenton and Richardson*, 2001b].

With the advent of mesoscale atmospheric models, the circulation of a small region can be examined in high-resolution detail for the first time. These models can be used in concert with spacecraft data, and in particular MOC NA (Mars Orbiter Camera Narrow Angle) images, which can provide detailed wind orientations at the scale of tens of meters. Comparing the two provides not only a verification of the mesoscale model and the GCM to which it is coupled, but also an understanding of the source of the winds that influence the surface. This in turn can lead to a better understanding of landscape morphology and the sources and sinks of mobile material. Recently, a mesoscale model has been applied over a crater and a valley, demonstrating that topographic and diurnal effects dominate the local windflow on Mars [*Greeley et al.*, 2001]. A mesoscale model applied over the Antarctic ice sheets has recently been used as an analog to the north polar residual ice cap on Mars in order to explain the presence of most of the surface features [*Howard*, 2000]. Mesoscale airflow has been modeled over a typical crater to show that the highest wind stresses correlate with the downwind crater rim, consistent with erosion patterns observed in small craters [*Kuzmin et al.*, 2001]. It
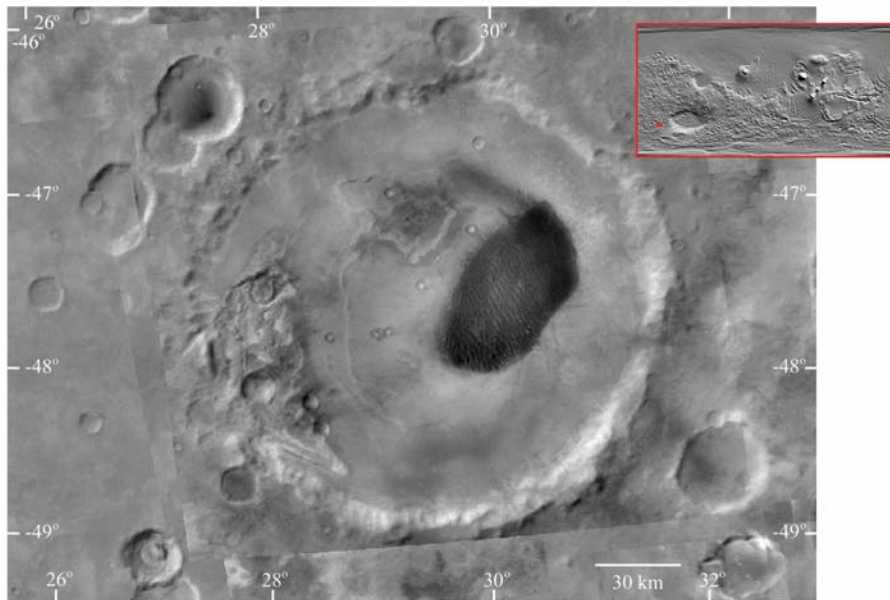
**Fig. 4.1.** Proctor Crater is a 150 km diameter crater with an interior dark dunefield, located in the southern highlands ~900 km west of Hellas Basin (see inset.)

has become clear that models with both higher spatial and temporal resolution are necessary to understand local and even regional wind patterns.

This work is the second of two papers describing aeolian processes in Proctor Crater, a 150 km diameter crater in the ancient cratered highlands of Noachis Terra (see Fig. 4.1). The first paper, *Fenton* [2003] (hereafter called Paper 1), discusses the morphology, composition, thermal properties, and stratigraphic history of the floor materials within Proctor Crater. With use of a number of different data sets in conjunction, it is shown in Paper 1 that the sedimentary history of Proctor Crater has involved a complex interaction of accumulating and eroding sedimentation. Aeolian features spanning much of the history of the crater interior dominate its surface, including large erosional pits, hundreds of meters of stratified beds of aeolian sediments, sand dunes, erosional and

depositional streaks, dust devil tracks, and small bright bedforms that are probably granule ripples. In this work we apply a mesoscale model to the atmosphere above Proctor Crater in order to determine how modeled winds correspond to the aeolian features described in Paper 1. First we review the orientations of aeolian features found in Paper 1, with an additional discussion regarding evidence for seasonally reversing slipfaces found in newly released MOC NA images. We then describe the mesoscale model and how the resulting wind predictions correlate to known surface features. We discuss seasonal and daily wind changes and the spatial variation of wind patterns on the Proctor Crater floor. Using sand grain density and particle sizes estimated in Paper 1 we discuss the likelihood of sand lifting under the predicted wind conditions.

## 2. MOC NA Observations of Proctor Crater Dunes

### 2.1 Measured Orientations

Wind orientations are visible in at least three different types of aeolian features: in the large dark dunefield in the center of the crater floor, in dust devil tracks that cover the floor during the spring and summer, and in small bright duneforms that are nearly ubiquitous on the crater floor. Each type of feature indicates a different time scale, indicating either recent or ancient winds. For example, dust devil tracks form and are subsequently obliterated each year, and therefore the winds that move dust devils downwind must be currently active. However, the large dark dunes may move on timescales of thousands of years or more, and thus may reflect older winds. Some of the bright duneforms may be ancient stabilized features, possibly indicative of winds dating to hundreds of thousands of years or more. Each type of feature and the wind information it provides is discussed in detail below. A summary of the results is presented in Table 4.1.

**2.1.1 Dark Dunes.** As discussed in Paper 1, the dark dunefield in the floor of Proctor Crater (see Fig. 4.1) displays three slipface orientations. Slipfaces are

**Table 4.1.** Current wind regime in Proctor Crater (based on MOC NA images)

| Wind | Locale | Features reflecting wind direction | Time of occurrence |
|---|---|---|---|
| Primary (WSW: 239° ± 18°) | Entire crater floor | Dune slipfaces, Bright duneforms | Fall and winter afternoon geostrophic-induced westerlies (strong) |
| | | Dust devil tracks | Sprint and summer early afternoon westerlies from planetary rotation (weak) |
| Secondary (ESE: 110° ± 18°) | Central and western portion of dunefield | Dune slipfaces | ? |
| Tertiary (ENE: 75° ± 9°) | Eastern portion of dunefield, possibly eastern portion of crater floor | Dune slipfaces, Bright duneforms (?) | Spring and summer evening katabatic flow (strong) |

produced by two processes. In the lesser process, grains are deposited by a sand-laden wind, coating the lee side of a dune. However, the morphology of the lee side of a dune is usually dictated by sand flow, produced by the avalanching of sand which is oversteepened by the downwind movement of sand from the stoss (windward slope). Continued avalanching produces the characteristic slipfaces that are used both to identify dunes and to determine the wind orientation, because slipfaces are always oriented transverse to the wind (*i.e.,* they dip downwind).

Figure 4.2a shows a rose diagram (*i.e.,* a histogram on a polar plot) of the measured slipface dip orientations, or downwind directions, from Paper 1. Each of the three slipface orientations is labeled with a mean and standard deviation formative wind orientation (note that although the rose diagram shows downwind slipface directions, following the geological convention, the labeled wind orientations refer to the upwind directions, following the meteorological convention). The three directions are labeled primary, secondary, and tertiary based on their spatial frequency within the dunefield. The primary dune slipfaces
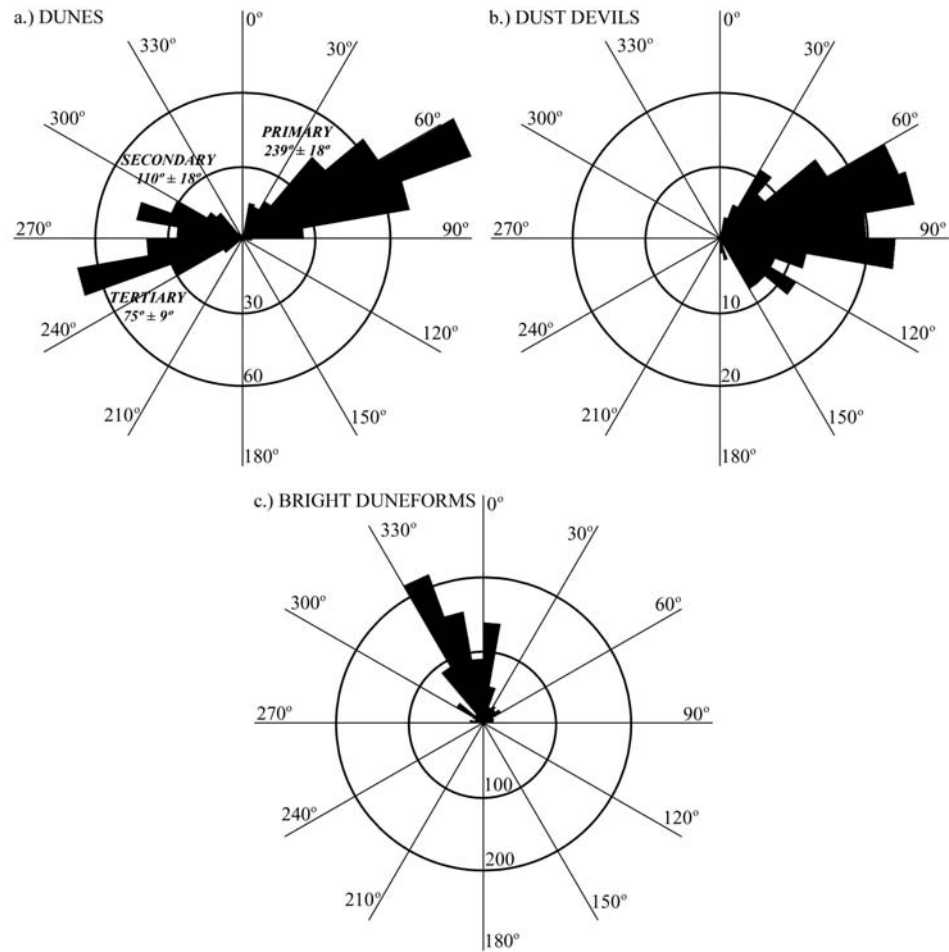
**Fig. 4.2.** Rose diagrams showing the azimuthal orientations of a.) dune slipfaces, b.) dust devil tracks, and c.) bright duneforms as measured in MOC NA images.

are created by winds from the WSW. These slipfaces are visible throughout the dunefield. Falling dunes on the eastern sides of hills and cliffs southwest (*i.e.,* upwind) of the dunefield are aligned with this wind, and have been interpreted in Paper 1 as the winds that carried the dark dune sand to its current location from the southwest. The secondary winds are consistent with winds from the ESE. They are prevalent throughout all but the easternmost portion of the dunefield, and dominate in the form of transverse dunes along the west-northwest edge of

the dunefield. A large dark streak of sand emanating from the northern tip of the dunefield is aligned with the secondary wind (see Fig. 4.1). The tertiary slipfaces indicate winds from the ENE. They are only present on the easternmost edge of the dunefield, where they are the principal dune-shaping winds. The tri-directional wind regime observed in the Proctor Crater dunefield is also a convergent wind regime, indicating that the dunefield resides in a location on the crater floor with zero or low net transport. As discussed in Paper 1, the transverse reversing and star dunes found in the dunefield are consistent with the observed convergent wind regime.

Individual images of dunes generally do not provide information on the season or local time of the winds that influence them. However, they do provide the orientations of the winds that last influenced them, which may indicate dune activity ranging from saltation up to and during the data acquisition to indurated surfaces that reflect ancient and now defunct wind systems. Therefore, in order to interpret the Proctor Crater dune slipface orientations in terms of the current wind circulation patterns, it must first be established that the dunes are currently active. The Proctor Crater dunes are free of dust accumulations that mantle the local surface each year, and although the surrounding crater floor becomes covered with dust devil tracks each spring and summer, the dunes display few such dust devil tracks. This suggests that the dunes are active, clearing away dust fallout with sand saltation, and that any dust devils that pass over dark sand leave behind no tracks because there is no dust left to be cleared away. Furthermore, the dune thermal inertia indicates the dunes are made of coarse-grained sand, consistent with previous measurements and predictions (see Paper 1). Thick dust deposits on the dunes would lower the thermal inertia to a value consistent with dust grains (besides being unlikely based on the low albedo of the dunes), and dune cementation would increase the thermal inertia to a value too large to be indicative of sand-sized grains. In addition, there are few if any indications of

hillslope erosion on the dunes or softening of slipface brinks, both of which are consistent with their being currently active. Thus the evidence suggests that each of the three measured slipface orientations corresponds to present-day winds.

**2.1.2 Dust devil tracks.** Dust devil tracks were identified in most of the spring and summer images on the Proctor Crater floor. They form first over dark patches of sand in the springtime, eventually spreading over much of the crater floor as the season progresses. Tracks overlap one another but generally are not erased within a single summer season. By the following year the tracks have been erased, indicating that fresh tracks form each year after new dust fallout has accumulated on the crater floor.

Most dust devil tracks are oriented WSW–ENE (see Fig. 4.2b). Because of a lack of obvious starting and ending points of the dust devil tracks, it is difficult to determine which direction the dust devils moved and thus the ambient wind direction in the early afternoon during spring and summer. No actual dust devils were imaged in Proctor Crater. However, as discussed in Paper 1, there is one springtime image showing dust devil tracks forming on a dark sand patch and moving downwind, pushed by winds from the WSW. Thus it is likely that all of the dust devil tracks, which form in the same season and during the same time of day, indicate winds from the WSW.

Dust devil tracks are visible throughout the spring and summer seasons in seventeen different images. It is possible that the mean wind direction drifts as the season progresses, perhaps reflecting changes in the strength of Hadley circulation or tidal flow. Thus we measured the mean orientations of the dust devil tracks as a function of $L_s$, including tracks from newly released images acquired during the second Martian summer. Where the dust devil tracks were plentiful, only the longest and most prominent tracks were measured. Where the

dust devils were faint and scarce, as was the case for all wintertime tracks, all visible tracks were measured. It is not clear whether tracks observed during the winter are fresh features or relics from the previous summer season. As a result, there is a measurement bias towards larger, longer-lasting dust devils during the spring and summer and towards small and potentially old tracks during the winter. The results are shown in Fig. 4.3, with small dots marking the orientation of individual dust devil tracks and large asterisks indicating the mean track orientation in each image. As with Fig. 4.2b, all tracks are assumed to be oriented
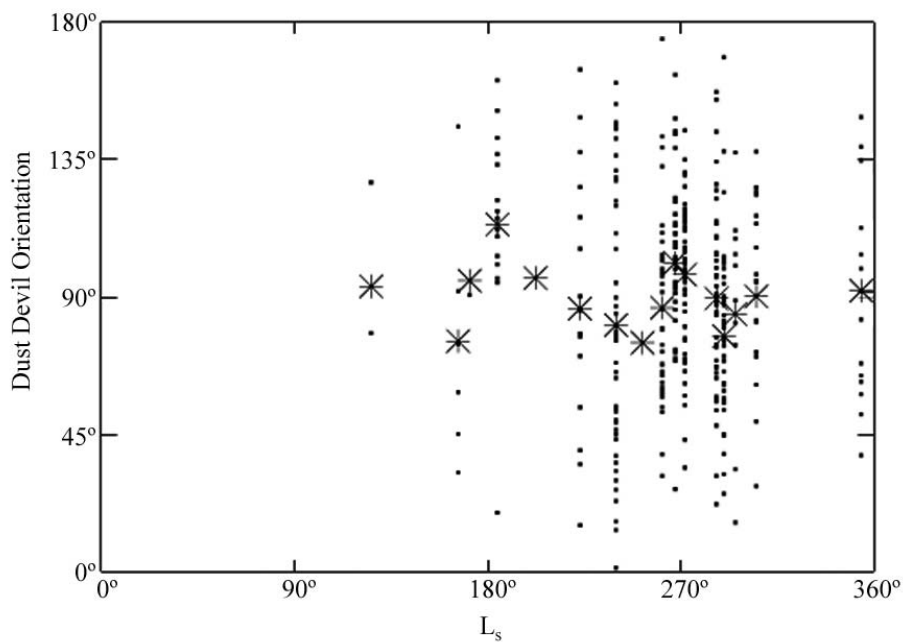


**Fig. 4.3.** Dust devil orientation as a function of season. Dots represent individual track orientations; large stars indicate mean orientations across a single MOC NA image.

between 0° and 180°, thus avoiding the directional ambiguity. Although there is a wide distribution is track orientations, they generally tend to cluster between 45° and 135°. The mean orientations in each image are always near 90°. Both of these observations are consistent with the WSW–ENE orientation shown in Fig. 4.2b.

Thus, according to the MOC NA images, there is no observable change in dust devil orientation in Proctor Crater during the year, indicating that the mean daytime wind direction during the spring and summer and possibly during the winter is fairly constant.

**2.1.3 Bright duneforms.** Bright duneforms cover much of the floor of Proctor Crater. They are visible in the interdunes in the large dark dunefield, indicating that these features were present before dark sand entered the crater. Although they are an order of magnitude smaller than the dark dunes, they are relatively immobile, indicating that they are either smaller stabilized dunes or very large granule ripples. The TES bolometric albedos of these features range from 0.12–0.14, making them "bright" relative to the dark dunes that have an albedo ranging from 0.06–0.12. For these reasons, they are referred to in this work as "bright duneforms" or "bright bedforms." They are most likely some sort of ripple, because there is an example shown in Paper 1 of a large dark barchan eroding bright duneforms as it slowly migrates by, only to have a few small features similar to the bright duneforms reform in its wake after it passed by. If these duneforms are in fact small dunes, then they would quickly migrate by the large dark dunes in an active wind regime. If most of the bright duneforms are simply stabilized dunes, then these features could not be recreated after being destroyed, as observed. Therefore these features are most likely very large granule ripples, which may migrate more slowly than dunes and yet still remain active.

The bright duneforms seem to be symmetric with no obvious slipfaces at the resolution of MOC NA images, making it difficult to determine whether they are aligned parallel or transverse to the local winds. Granule ripples tend to be transverse to the wind [*Sharp,* 1963], so if these features are ripples, as proposed, then they are probably transverse as well. Figure 4.2c shows a rose diagram of the along-crest direction of the bright duneforms. If they are transverse then they

were formed by winds from either the WSW or the ENE. These directions are consistent with both the primary and tertiary slipfaces found in the dark dunes. It is possible that where the primary winds dominate, the bright duneforms were created by winds from the WSW, and that where the tertiary winds dominate, the bright duneforms were created by winds from the ESE. Some of the bright duneforms may be ancient features, far older than the dark dunefield. If this is the case then they reflect ancient winds, indicating that wind circulation patterns have changed little since they were created.

## 2.2 Annual Slipface Reversal

Although dune slipface orientations show the predominating wind directions that influence the dunefield, they do not indicate the season or time of day in which these winds blow. In fact, without evidence for recent dune movement, it is difficult to prove conclusively that these slipfaces were not formed by ancient winds that no longer blow, and that the dunes are not largely dormant. The paucity of erosional features on the dunes supports the idea that the dunes are not stabilized, relic features. In addition, movement of dunes the size of those in the Proctor dunefield could take a century or more to identify using data with the currently available image resolution, and thus their lack of movement cannot be used to conclude that they are stabilized.

However, there is evidence for slipface reversal in dunes on the eastern edge of the Proctor dunefield that clearly indicates dune activity within the timespan of the MGS mission. The eastern portion of the dunefield consists of relatively smaller dunes with visible interdune areas, in contrast to the huge dunes atop the 50 m deep mound of sand found in the central and western-central portions of the dunefield (see Fig. 12 of *Fenton* [2003]). The eastern part of the dunefield is likely a younger offshoot of the main accumulation of sand. At some point, winds from the southwest (the primary winds) blew sand from the main dunefield to

the northeast, where it halted upon encountering east-northeasterly winds (the tertiary winds), which only influence the eastern part of the dunefield. Here the dark sand is largely balanced between the primary and tertiary winds, producing reversing transverse dunes common to the dunefield.

In Paper 1, bright material was described on slipfaces of double-sided barchans at the eastern edge of the dunefield. This bright material was attributed to the erosion of nearby underlying bright bedforms, which have a rounded appearance consistent with deflation and abrasion. It is only off the eastern edge of the dunefield that the bright bedforms have this rounded appearance, and it is only at the eastern edge of the dunefield that the dark barchans display bright slipfaces. This bright material cannot be residual frost because it is visible even in summertime images, when the surface is far too warm to support either $CO_2$ or $H_2O$ frost.

The slipface containing bright material switches sides of the double-sided barchans, as shown in Fig. 4.4. Figure 4.4 compares two overlapping MOC Narrow Angle images of the same area at different times of the year. Figure 4.4a shows mid-fall frosted dune surfaces with bright material on northeast slopes. Figure 4.4b shows an overlapping image from the following year during the late spring, with fully defrosted dune surfaces bearing bright material on western slopes. Note that although the solar azimuth is similar in Figs. 4.4a and 4.4b, the solar altitude is much higher in Fig. 4.4b leading to fewer shadows and an increased emphasis on albedo contrast. The albedo contrast in Fig. 4.4b is enhanced by the lack of frost cover present in Fig. 4.4a. Figures 4.4c and 4.4d illustrate the slipface brinks and accumulations of bright material with colors corresponding to the formative wind directions (yellow is primary, magenta is tertiary). Figure 4.4e shows both slipface directions, emphasizing that they are on
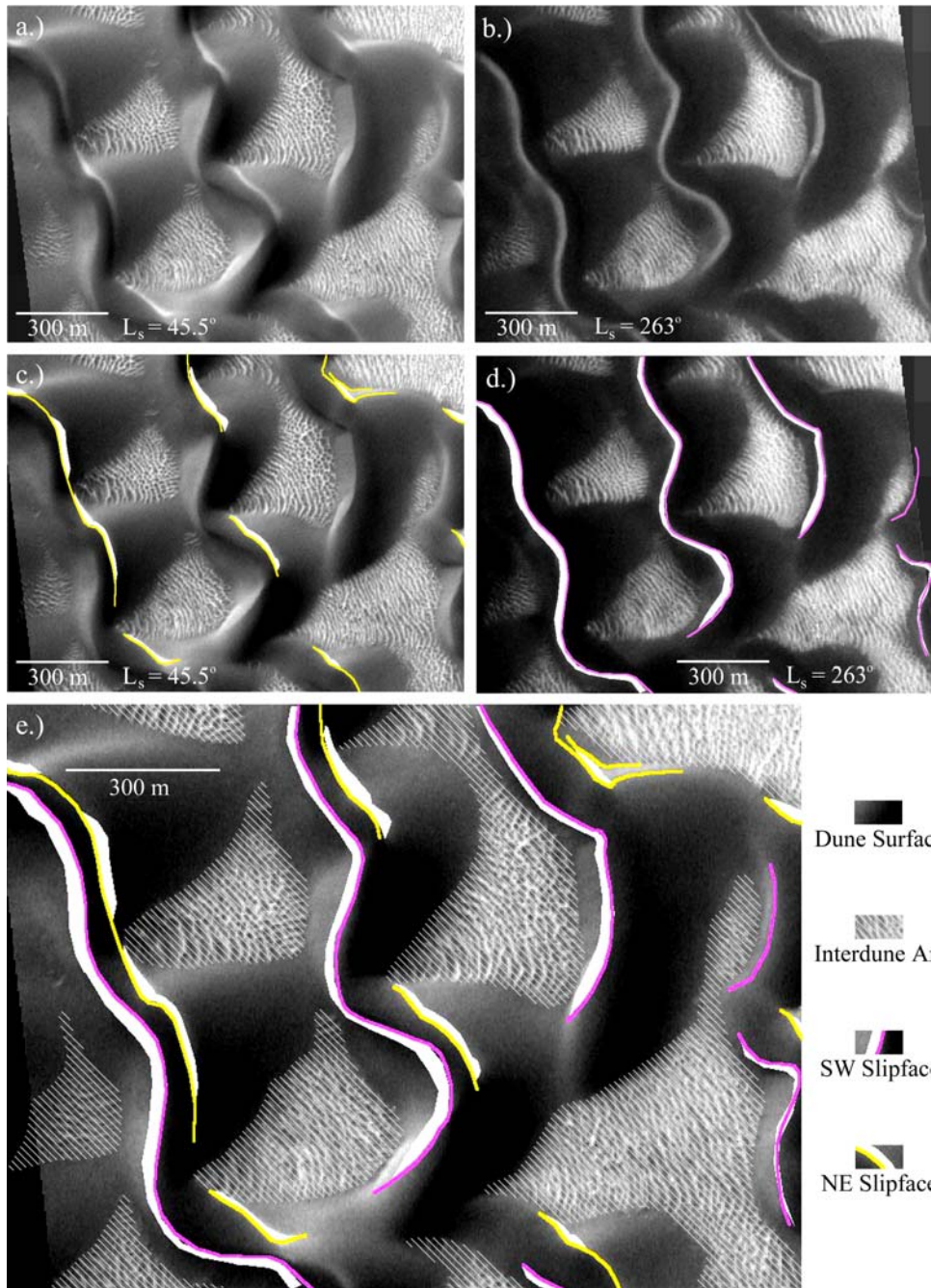
**Fig. 4.4.** Reversing slipfaces on dunes at the eastern edge of the dunefield. a.) MOC NA M1900307 during the fall and b.) MOC NA E0902707 during the spring show the same area with bright accumulations on opposing slipfaces. c.) and d.) illustrate the locations of slipface brinks and bright accumulations. e.) shows both sets of slipfaces and bright material. Note the slight shifting of one slipface brink in the upper right.

opposite sides of the barchans. Typical terrestrial reversing dunes switch sides with opposing seasonal winds, erasing the old slipface from the preceding season. The dunes in Proctor Crater display both slipfaces at different seasons, indicating that the slipfaces are not fully erased by opposing winds, leading to seasonally activated slipfaces. The fact that seasonal slipfaces are not fully erased may be caused by some amount of internal cementation of the dune, or by the fact that the slipfaces are too large to be demolished in a single Martian season.

In Figure 4.4c, one dune in the upper right corner of the image has two slipface brinks drawn on it. The more southwesterly and larger slipface corresponds to that in Figure 4.4a, and the smaller and more northeasterly brink corresponds to that in Figure 4.4b. This shift in slipface position probably indicates movement of this slipface toward the northeast between mid-fall and the following spring, although the dune itself has not shifted position. This movement indicates a shift of 13 to 37 m, depending on where along the brinks the movement is measured. Such a shift indicates strong and persistent seasonal winds. No other slipfaces in the frame moved and no dunes changed position, suggesting that movement of this type is rare.

Figure 4.4 indicates that between mid-fall and late spring, the prevailing winds change direction and that both winds influence the dunes. Bright material is likely blown from the stoss (upwind) slope onto the slipface along with any loose dark sand from the dune surface. If the dark sand on the dunes is mobile then an explanation must be found for why mobile bright material does not mix with the dark sand as it moves back and forth over the dune. Rather, the bright material remains on the surface, unmixed and unburied. It is possible that the dark sand in the dune is somewhat indurated, and that only the bright sand is moving back and forth as the seasons progress. However, the thermal inertia of the Proctor Crater dunes is consistent with loose, coarse sand (see Paper 1 and references

within). It is more likely that some amount of dark sand moves back and forth over the dune as the winds shift, but that the bright material is more easily mobilized by the wind, and thus is the last to settle onto the slipfaces as the winds decrease. This may indicate that the bright saltating material is made of smaller or less dense particles, causing them to saltate under lighter winds than the coarse basaltic grains comprising the dark sand.

Six MOC Narrow Angle images pass over the eastern edge of the Proctor Crater dunefield, imaging slipfaces at different seasons. Following the hypothesis that the bright material accumulates on the downwind side of the dunes, the dunes in this region are influenced currently by the primary and tertiary winds. Figure 4.5 shows each inferred wind orientation as a function of $L_s$, labeled by the MOC
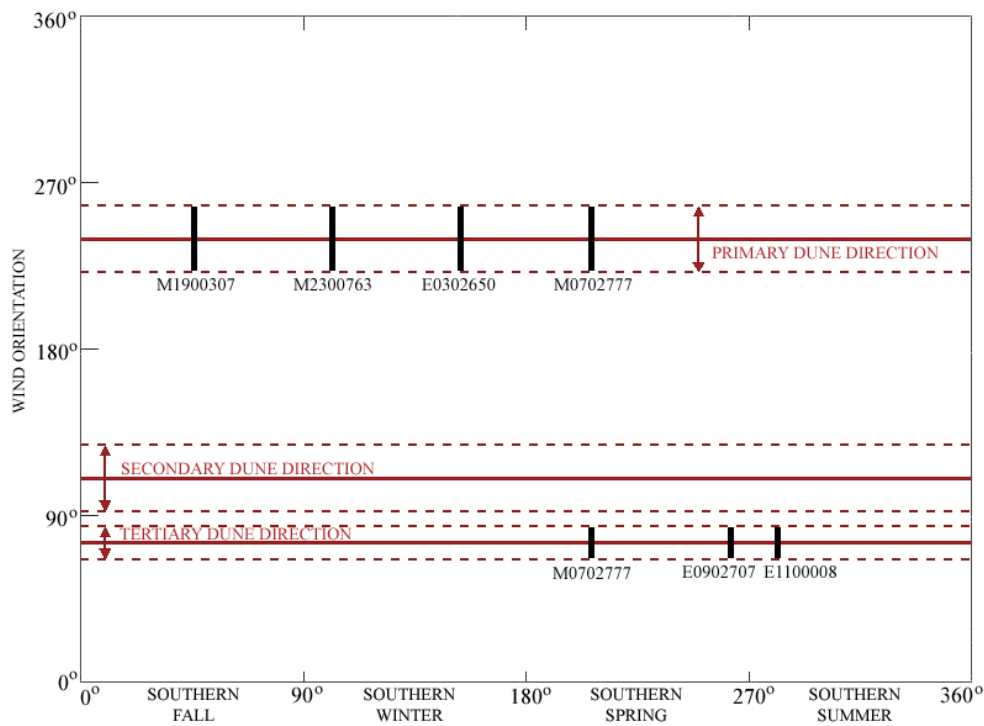


**Fig. 4.5.** MOC NA frames showing accumulations of bright material on oppositely oriented slipfaces. Horizontal red lines correspond to the three dune slipface orientations.

NA frame in which it was found. The red lines mark the three mean and standard deviation dune slipface directions. Reading from this plot, the primary slipfaces are active throughout fall and winter, and the tertiary slipfaces are active during spring and summer. MOC frame M0702777 from $L_s$ = 206.68° appears to have bright material on both slipfaces, and likely indicates a transition time between the two seasonal wind regimes. As discussed next, the modeled winds reflect the activity of these slipfaces.

## 3. Mesoscale Modeling of Surface Winds

### 3.1 The Mars MM5

Mesoscale atmospheric models are tools that have recently been made applicable to Martian conditions. These models function similarly to Mars GCM's, but they can examine atmospheric patterns that vary from the synoptic (1000's km) down to the microscale (10's m). The goal of applying a mesoscale model to Proctor Crater is to determine how well predicted wind directions correlate with dune slipface orientations.

We applied the Mars MM5, developed from the PSU/NCAR 5th Generation Mesoscale Model (MM5) by *Toigo* [2001]. The model is nonhydrostatic and uses terrain-following sigma coordinates. Initial and boundary conditions are provided by the Geophysical Fluid Dynamics Laboratory (GFDL) Mars General Circulation Model (GCM), which inherently couples the Mars MM5 to the GCM. The boundary layer parameterization scheme used in the Mars MM5 is that used in the Medium Range Forecast (MRF) [*Hong and Pan,* 1996], which has been modified for Martian surface conditions [*Toigo,* 2001].

Most of the Martian-specific parameterizations used in the Mars MM5 are taken directly from the GFDL Mars GCM. Radiative transfer is modeled using the scheme of *Wilson and Hamilton* [1996], which involves solar absorption by $CO_2$

and atmospheric dust of two particle sizes. The surface is represented by a MOLA topographic map [*Smith et al.,* 2001]; albedo maps by *Pleskot and Miner* [1981], *Paige et al.* [1994], and *Paige and Keegan* [1994]; and thermal inertia maps from *Palluconi and Kieffer* [1981] and *Vasavada et al.* [2000]. Ground temperatures are calculated using a 12-layer subsurface heat diffusion model that uses initial temperatures from the GCM.

We ran twelve 10-day simulations equally distributed around the Martian year. Twenty-four pressure levels were defined, from near the surface (~50 m height) to the top at ~80 km above the surface. Horizontally, we used a 50 x 50 horizontal point grid with a resolution of 10 km. The grid was centered on Proctor Crater and it extended more than one crater diameter in each direction to avoid potential edge effects. The timestep used in the simulations was 5 seconds, and parameters such as wind velocity and stress were saved once every hour as instantaneous values. In the past, hourly averaged values have been commonly used to provide a representative set of parameters. However, in this case the instantaneous values at the top of each hour were used instead to avoid washing out varying parameters that can be caused by using mean values.

## 3.2 Model Results

**3.2.1 Seasonal Winds.** Because the strongest daily winds are those that will move the most sand, it is these winds that will most affect dune morphology. Therefore we first discuss the orientations of the winds with the strongest daily stresses. These maximum winds are shown in Fig. 4.6 as a function of $L_s$ and wind orientation. Daily maximum winds are indicated by black boxes with sizes that correspond to wind stress, which is discussed in more detail in Section 3.2.3. The time of year included in each model run is shown as a blue shaded strip. The three mean wind directions observed in the dunefield and their standard deviations are indicated and labeled in red.

The strongest daily winds shift in direction with the seasons. Fall and winter winds come from the west and west-southwest. Spring and summer winds blow from the east-northeast, but they are weaker than their fall and winter counterparts. The fall and winter winds correspond well with the primary dune slipfaces, and they are most likely responsible for both the dune slipfaces and the
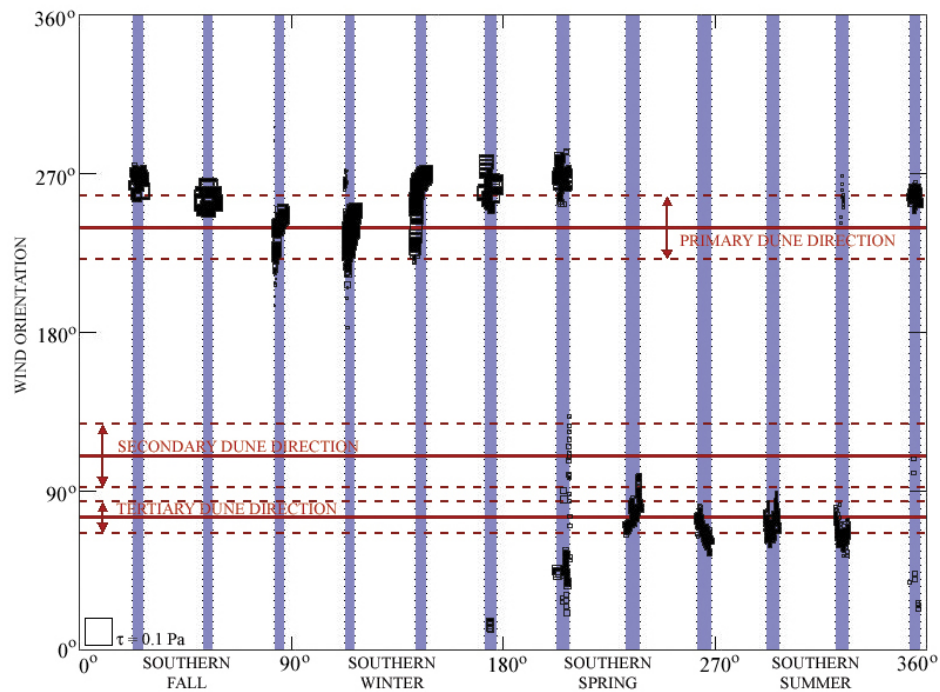


**Fig. 4.6.** Maximum daily stresses from model grid points located on the dunefield. The symbol size indicates magnitude of stress. Horizontal red lines correspond to the three dune slipface orientations.

orientations of most of the bright duneforms that are common on the Proctor Crater floor. The timing of the strongest winds compares well with the slipface reversal (compare Figs. 4.5 and 4.6). Even the MOC NA frame M0702777 that shows bright material on both slipfaces coincides with the season at which the

strongest daily winds switch direction, indicating that this image has caught the dunes during a transition from one wind regime to the other.

Dust devil tracks are also aligned with the primary wind, but they are generally only visible in spring and summertime images, indicating that this fall and winter wind is not responsible for creating the majority of dust devil tracks. The dunes do become covered in $CO_2$ frost during the winter, which may inhibit sand activity, precluding the winter winds from producing slipfaces. However, MOC NA images show fully frosted dunes only for the time period between $L_s = 50°$– 145°, with partial frost lasting until $L_s = 165°$. According to the model results in Fig. 4.6, the primary winds blow from $L_s = 350°$ to 200°. Therefore even if the frost cover temporarily stabilizes the dunes, the winds before and after the period of frost cover may account for the observed dune activity.

The winds in general are stronger during the winter, which likely indicates why they produce the most common slipfaces in the dunefield. However, the tertiary winds appear to dominate on the eastern edge of the dunefield, where these slipfaces are larger and the outlines of the barchan dunes appear to emphasize the tertiary winds. Further examination of the physics of saltation may explain why the tertiary winds have more control over the dunes they affect than the primary winds (see Section 3.2.3).
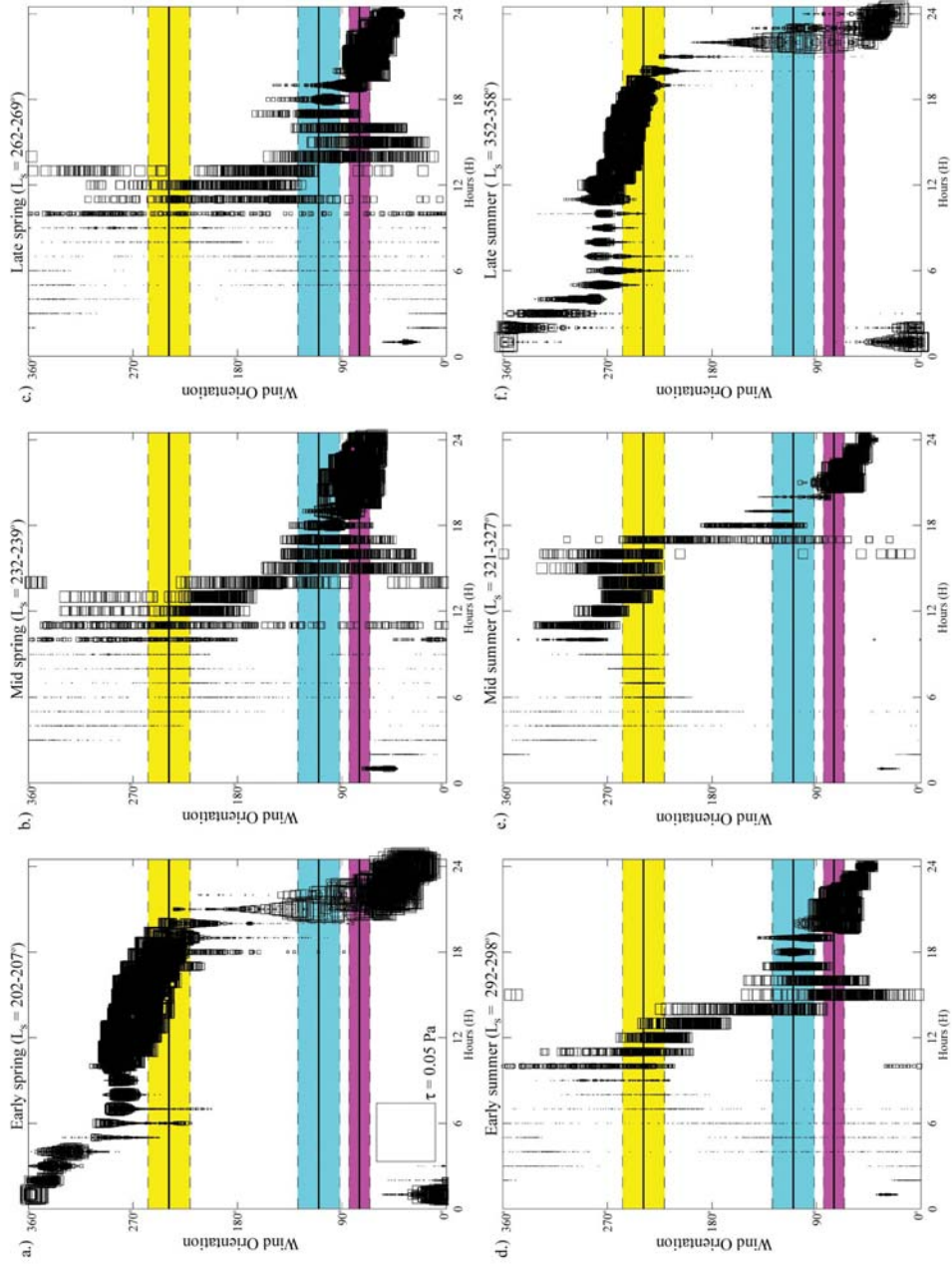
The secondary winds, from the ESE, are absent from Fig. 4.6. They are also absent from the dunes in Fig. 4.4, but this is on the eastern edge of the dunefield where slipfaces oriented with secondary winds are not present. It is not clear why the ESE winds do not appear as the strongest winds at some point of the year, but it may be that they are produced by slightly weaker winds at some point during the day that does not appear in Fig. 4.6. Therefore, before we can state

that the model does not predict the secondary winds, we must discuss wind orientation and strength as a function of time over the course of the day.

**3.2.2. Daily Winds.** To understand changes in winds during the day, we saved hourly winds when running Mars MM5 over Proctor Crater. The strongest daily winds correspond to two of the three observed dune slipface directions, but they do not explain the missing secondary winds that produce another dune slipface direction in the dunefield. They also do not explain the orientation of dust devil tracks during the spring and summer, which seem to be oriented 180° from the strongest winds during that season. Hourly winds during each model run show much more detail than in Fig. 4.6. The origins of the observed winds are discussed below in Section 3.2.4.

Figure 4.7 shows the orientation of winds over the Proctor crater dunefield for each hour in each model run. A total of twenty-five grid points in the model were located over the dunefield, and each point is plotted in Fig. 4.7. As with Fig. 4.6, the three mean and standard deviation slipface directions are marked, and the black boxes indicating modeled winds are scaled by wind stress. Each model run is shown separately and labeled, although all ten days included in each run are shown in a single plot. Spring and summer model runs clearly show tertiary winds during the evening hours, and WSW winds during the daytime. The evening winds are the strongest winds of the day, as shown in Fig. 4.6, but the early afternoon winds correspond well with the dust devil track orientations.

Fall and winter winds that are aligned with primary winds are the strongest of the year, and they blow during the afternoon. Winds from the WSW occur throughout the year, but they become much stronger during the fall and winter. Thus a weak WSW produces dust devil tracks during the spring and summer, and a strong WSW wind creates slipfaces during the fall and winter.
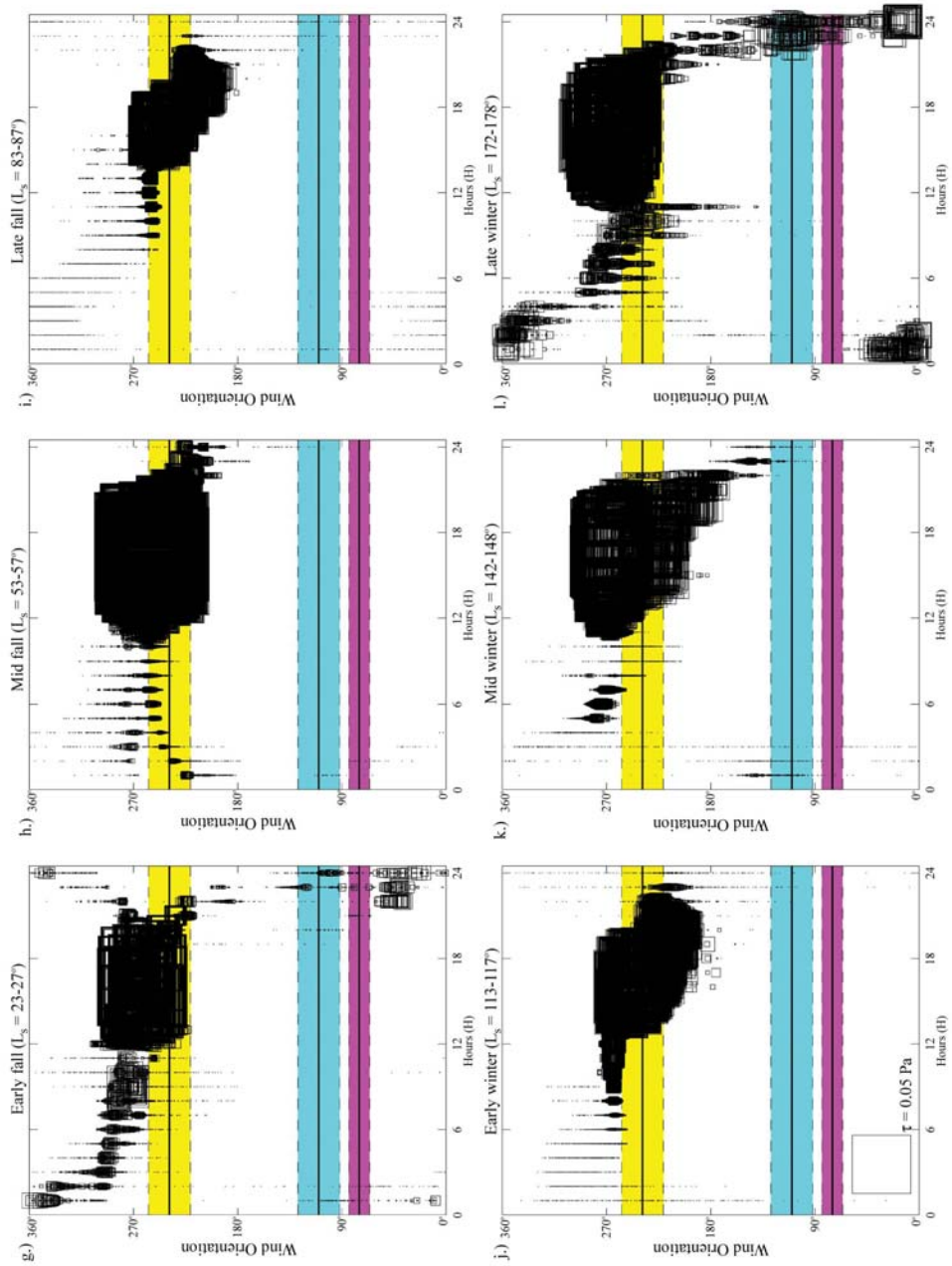
**Fig. 4.7.** Modeled hourly wind orientations over the dunefield for each model run. Data symbols are scaled by the magnitude of stress.

None of the daily winds indicate any alignment with slipfaces oriented to secondary winds, suggesting that perhaps these winds no longer blow. However, the slipfaces made by ESE winds are crisp and uneroded, implying that they probably not relics of an old wind regime. There are winds that briefly align with these secondary winds during the time of transition between the winter and summer circulation patterns (see Fig. 4.7 at $L_s = 352°–358°$ and $172°–178°$) and in the late afternoon during the summer (see Fig. 4.7 at $L_s = 232°–239°$, $262°–269°$, and $292°–298°$). But these winds are not strong and do not appear to be part of any persistent and unidirectional wind pattern. It may be that a full year's run would produce a time when the secondary winds dominate, although the model runs here appear to be fairly representative of modeled winds throughout the Martian year.

**3.2.3. Wind Stresses.** Although the modeled winds may align with observed wind features, only winds above a particular threshold stress value are strong enough to initiate saltation. Some wind features, such as dust devil tracks, do not rely on sand saltation, and in these cases the modeled stress is not a directly relevant parameter. However, saltation initiation is important for explaining features such as dunes, which are morphologically controlled solely by sand saltation. *Iversen and White* [1982] conducted wind tunnel experiments, finding an empirical relation for the saltation threshold under Martian atmospheric conditions. They found that the threshold varied as a function of particle size, particle density, atmospheric temperature, and atmospheric pressure. Because the saltation threshold is sensitive to so many parameters, it is crucial to constrain these values in order to determine whether the mesoscale model truly predicts the saltation of sand within the Proctor Crater dunefield.

In Paper 1, thermal inertia values derived from TES led to an estimated effective sand grain size for the Proctor Crater dunes of $740 \pm 170\,\mu m$. In addition, the

compositional analysis described in Paper 1 indicated that the dunefield is almost exclusively composed of basalt grains, where the basalt is inferred from the identification of pyroxene and plagioclase in TES spectra. In this work we assume the grains have a density typical of terrestrial basalt (3200 kg m$^{-3}$), although it is possible that the sand could be composed of grains with a lower bulk density (*e.g.,* scoria). Modeled surface air pressures and air temperatures vary with local time and season. In the early afternoon during the southern winter solstice, when the primary winds dominate over all other winds crossing the dunefield, the air temperature is ~155 K and the air pressure is 6 mbar. In the evening hours during the southern summer solstice, when the tertiary winds blow, the air temperature is ~235 K and the air pressure is 6 mbar. It is interesting to note that the daytime winter air pressure is roughly equivalent to the evening summertime air pressure. Figure 4.8a shows the saltation stress threshold for 740 µm diameter basalt grains at an air pressure of 6 mbar as a function of near-surface air temperature based on the relation by *Iversen and White* [1982]. The upper curve indicates the fluid stress threshold, or the stress required by the air alone to lift grains in to saltation. The lower curve indicates the impact stress threshold, or the stress necessary to saltate grains from the impact of already saltating grains. The impact stress threshold may be considered roughly equivalent to ~0.8 that of the fluid stress threshold [*Bagnold,* 1941; *Andersen and Haff,* 1988; *Toigo et al.,* 2002a]. Because movement from such impacts is the mechanism that causes most grains to saltate, the impact stress threshold is considered to be the most representative threshold stress value. Figure 4.8a shows the estimated threshold stress values for typical conditions under which both the primary and tertiary winds blow. In the winter the stress required to lift the dune sand is 1.5 times that required in the summer, indicating that conditions leading to saltation vary with the seasons in Proctor Crater. This difference may explain why the tertiary winds dominate over the primary winds in dune morphology on the eastern edge of the dunefield, as
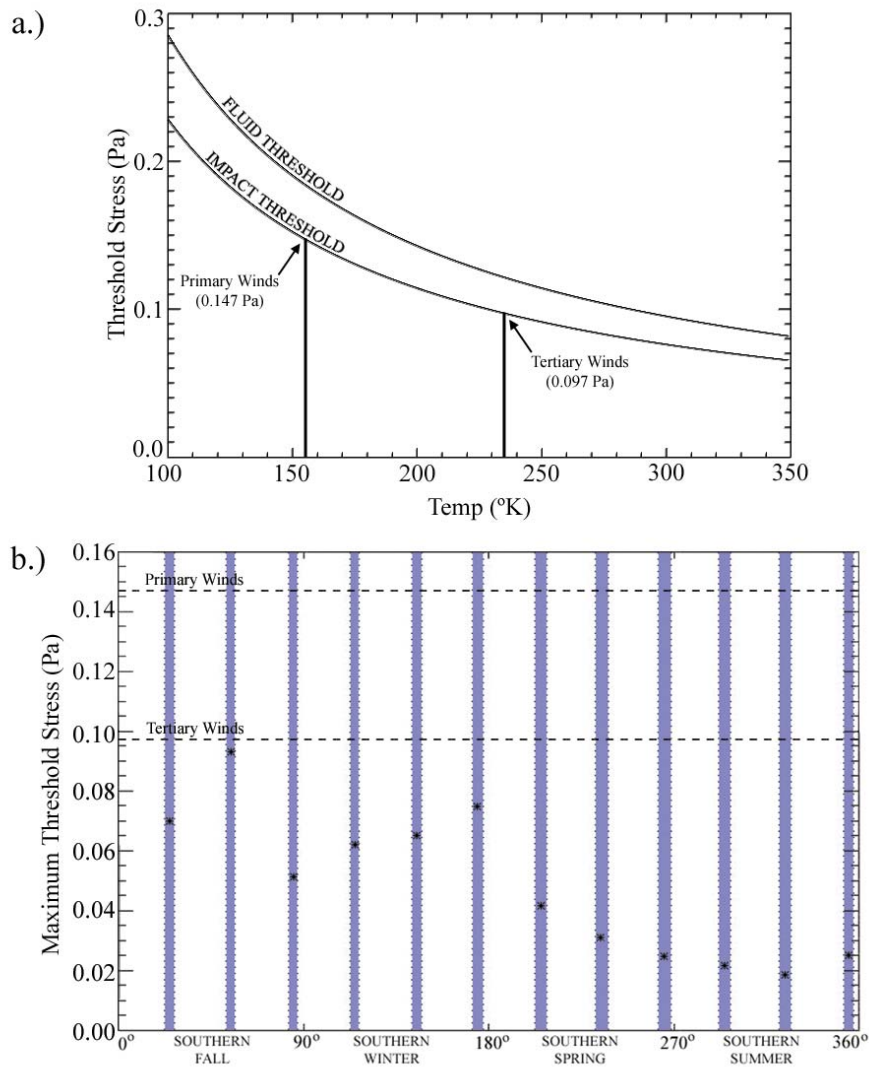
a.)



b.)



**Fig. 4.8.** a.) Saltation threshold as a function of air temperature. Note the difference in threshold stress values between the primary and tertiary winds. b.) Maximum predicted stresses over the dunefield in each model run.

discussed in Section 2.1.1. Even though the winter winds are stronger than the summer winds that are aligned with the Tertiary slipfaces (see Fig. 4.7), the lower threshold stress during the summer suggests that these winds may be relatively more effective in moving sand.

Although winds predicted by the Mars MM5 are well aligned with two observed slipface orientations, the calculated wind stresses are not high enough to predict sand saltation. Figure 4.8b shows the maximum calculated wind stresses over the dunefield in each of the twelve model runs. Even though the winter winds are the strongest of the year, they are still not above the lower summertime saltation threshold. There are a number of reasons why the model may not be predicting winds that are strong enough to saltate sand. The first and most obvious reason is that the grid spacing of 10 km by 10 km is too large to capture local wind gusts, with each grid point representing an average predicted wind over a 100 km$^2$ area. This is a problem that has plagued modelers applying GCM wind predictions to sand saltation [*e.g., Greeley et al,.* 1993; *Anderson et al.,* 1999; *Toigo et al.,* 2002b]. A recent sensitivity study of model resolution in a terrestrial mesoscale model indicates that predicted wind stresses are more accurate at higher resolutions in which the topography is better defined [*Liu and Westphal,* 2001]. Thus model resolution appears to be a significant factor in predicting wind strength, and this may be the case for our model runs as well. A second possibility is that during the model runs, although the timestep was 5 seconds, we only outputted winds from the top of each hour to conserve disk space. It may be that winds above the saltation threshold would have been captured if instead the strongest winds of each hour were considered, because rare wind gusts may produce saltation. We consider the 10 km scale of the model runs in this work to be the source of the problem of weak winds.

**3.2.4. Spatial Variation and Origin of Wind Orientations.** The primary winds appear to influence dunes, falling dunes, and bright duneforms throughout the interior of Proctor Crater. The tertiary dunes only affect the eastern edge of the dunefield and perhaps the orientations of some of the bright duneforms in the eastern portion of the crater floor. Modeled winds should reflect this pattern if they truly represent actual surface winds.

Figure 4.9 shows two maps of instantaneous winds. The winds are superimposed on a MOLA elevation map, with violets and blues indicating low elevations. The dunefield is visible as a lighter blue mound at 30.2º E, -47.7º S. Figure 4.9a shows afternoon winds during fall, when the primary winds blow (see Fig. 4.7). The arrows represent the velocities of the lowest-level winds, at a height of ~250 m. The winds across the whole area are oriented from the WSW, indicating that the primary winds do in fact influence the entire crater floor. These fall and winter winds are simply midlatitude westerlies created by a geostrophic force that is strengthened by the strong latitudinal temperature gradient present in the winter hemisphere. The slight deflection to the south is caused by the presence of the Hellas basin some 900 km to the east, which warps the approaching winds.

Figure 4.9b shows another wind map, this time from the early evening hours during the spring. Strong winds from the east-northeast dominate the eastern portion of the crater. These are the tertiary winds that control dune morphology on the eastern edge of the dunefield. As the evening progresses, the ENE winds sweep across the crater floor until they are the sole winds blowing in this area, but the fact that they blow for a longer period of time in the eastern part of the crater floor likely explains why they are only visible there. This set of winds is caused by the diurnal tide, in which winds east of the subsolar (noonday) point surge towards this point to fill the vacuum caused by rising air in the summer noontime heat. Furthermore, as the ENE winds cross the eastern rim of Proctor Crater, they encounter relatively warmer air rising from the crater floor ~1500 m below. The air spills beneath this lighter air into the crater in a katabatic flow, accelerating down and across the crater floor. It is these winds that explain why sand has become trapped in Proctor Crater: the primary winds blew sand into the crater from the WSW, but the sand stopped when it encountered the tertiary winds from the ENE that effectively stop dune migration to the east. Sand outside the crater does experience ENE winds at this time of year, but on the
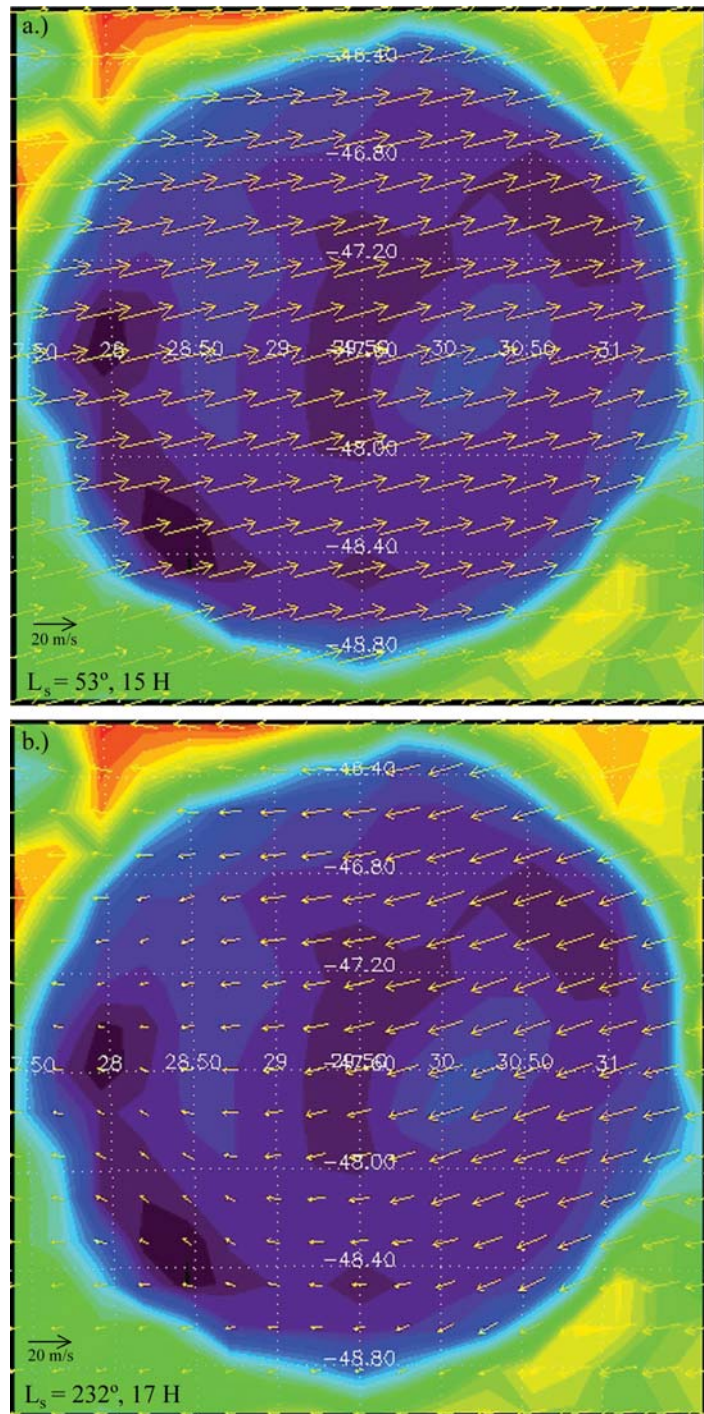
**Fig. 4.9.** Surface wind vectors illustrating a.) primary winds during the afternoon in the fall and b.) tertiary winds in the evening during spring. The dark dunefield is indicated by a local topographic high at 30.2° E, -47.7° S.

intercrater plains these winds are not enhanced by topography as they are in the floor of Proctor Crater, and so sand did not accumulate on the intercrater plains. Material that was not trapped in craters in Noachis Terra most likely continued to migrate downwind and was likely trapped in the Hellas basin to the east.

Another way to show the spatial distribution of wind orientations across the dunefield is to show rose diagrams for each grid point in the model run. Figure 4.10a shows a rose diagram for each such grid point summed over each of the twelve model runs. The histograms show frequency of wind orientation without regard to wind strength, and thus they emphasize wind persistence. The outer white ring outlines the Proctor Crater rim, and the smaller inner ring defines the edge of the dunefield. Like the histograms of surface feature orientations, these rose diagrams show the downwind direction (for example, an accumulation of winds oriented to the north in these diagrams indicates winds blowing from the south). In most areas of the crater floor, winds from the WSW dominate over all other wind directions throughout the year. In no cases are secondary winds, from the ESE, present in any quantity. In the northwest and southeast edges of the crater floor, a northwesterly wind predominates, but it is not reflected in any observed aeolian feature on the surface. These winds are likely too weak to carry sand or scour material from the surface, but they do occur frequently enough to appear on this figure.

A better way to emphasize the variation in wind variation is to subtract from all grid points the histogram from a single control grid point. Figure 4.10b shows the cumulative winds at each grid point minus the winds at the control point, which we chose from the center of the dunefield (marked in boldface). Thus all of the differenced rose diagrams show winds with respect to those predicted over the center of the dunefield.  Note that the scale of the histograms, marked on the left, varies from one plot to the next. Compared to Fig. 4.10a, the variation in wind
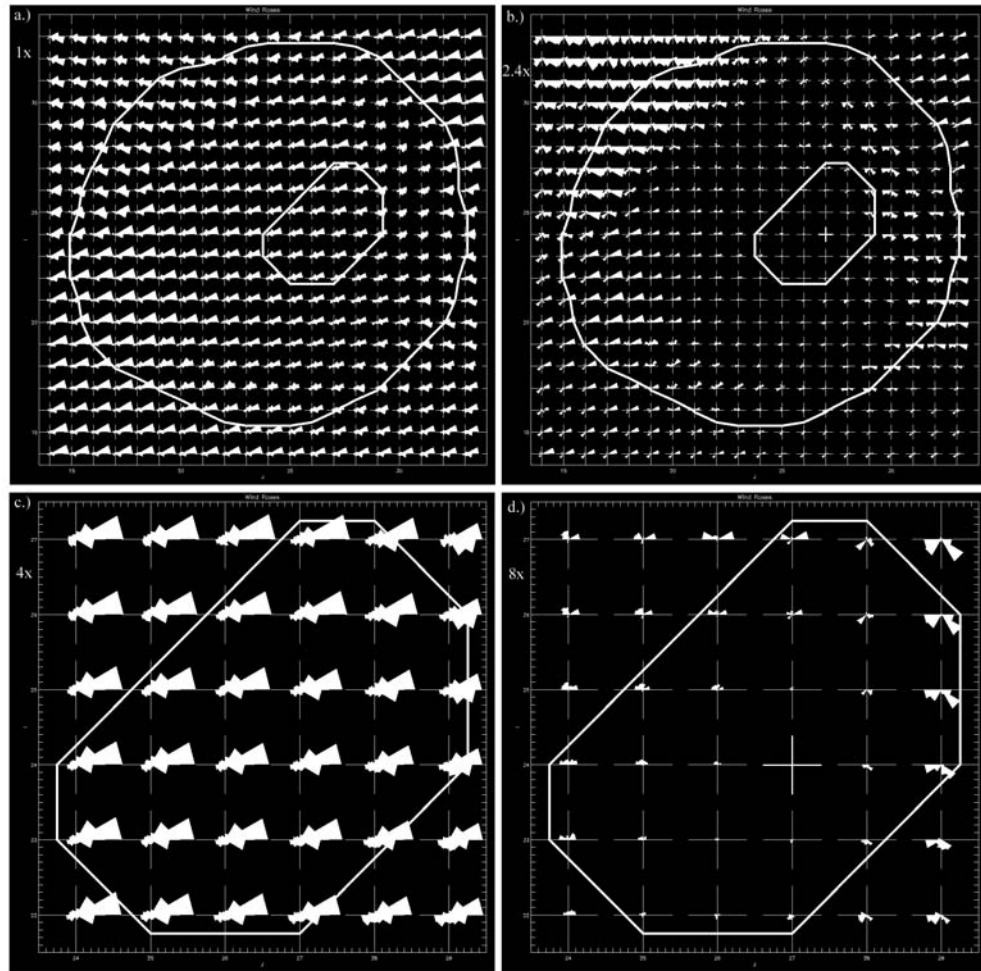
**Fig. 4.10.** a.) Rose diagram of all wind orientations in all model runs for each grid point across the crater, and b.) the same differenced with a control rose diagram from the center of the dunefield (marked in boldface). The crater rim and dunefield are outlined in white. c.) and d.) show the same as a.) and b.), zoomed in on the dunefield. Note that these diagrams indicate downwind direction.

orientation from point to point in Fig. 4.10b is much more visible. The center of the crater has winds fairly similar to those observed on the dunefield. The northwesterly winds at the northwestern and southeastern edge of the crater are much easier to discern. Tertiary winds from the ENE are clearly more common in the eastern portion of the crater floor, precisely where aeolian features in MOC images indicate that they exist. The primary winds are more persistent at the edge

of the crater, in the southeast, than elsewhere, which may indicate that more erosion and sand migration is occurring near the edge of the crater floor than downwind near the dunefield.

Figure 4.10c shows summed rose diagrams for all model runs over the dunefield, with the dunefield outlined in a thick white ring. The dunefield itself shows rose diagrams that appear to vary little from point to point. The primary winds, from the WSW, are clearly the most frequent winds that blow over the dunefield. When the control point is subtracted from the rose diagrams, more detail appears (see Fig. 4.10d). The tertiary winds from the ENE influence the eastern portion of the dunefield, which is consistent with the distribution of the tertiary dune slipfaces. The northwesterly wind that appeared in Fig. 4.10a and 4.10b appears again on the eastern edge of the dunefield, again reflecting frequent but weak winds that cannot saltate sand.

On the northwest edge of the dunes, there are signs of winds that are aligned with the mysterious secondary winds. This is the portion of the dunefield in which the secondary-facing dune slipfaces dominate. The ESE winds in Fig. 4.10d are caused by winds in transition from one dominant direction to another. For example, modeled winds correlate with the secondary winds in the late afternoon during spring and summer as winds shift from the early and mid afternoon WSW winds that produce dust devil tracks to the evening ENE tertiary winds (see Fig. 4.7b–d). In addition, modeled winds aligned with the secondary winds occur in the evening during the seasonal transition from the winter to summer wind regime (see Fig. 4.7a and 4.7l) and again during the transition from the summer to the winter wind regime (see Fig. 4.7f). The winds are not strong in either case, and they do not persist in the direction of the secondary winds for any length of time. Thus although some winds aligned with the secondary winds

are predicted by the model, they are not likely responsible for forming the observed slipfaces.

## 4. Discussion and Conclusion

The Mars MM5 model runs predict and explain the wind patterns behind two of three observed dune slipface orientations as well as dust devil track orientations. However, it does not produce winds matching a third dune slipface orientation of any strength or duration. One possible explanation for the missing secondary winds is that the Mars MM5 model runs covered too small a domain and thus did not account for regional effects that might influence wind directions, such as the deep Hellas basin 900 km to the east. One way to check for such an inconsistency is to compare the Mars MM5 results to those from a GCM.

The primary and tertiary winds, as well as the WSW summer winds that produce dust devil tracks, are visible in GCM wind predictions as well as in Mars MM5 model runs. *Fenton and Richardson* [2001b] made global predictions of surface winds using the GFDL Mars GCM. The average southern fall and winter winds at the location of Proctor Crater (47.5º S, 30º E) are from the WNW to WSW, fairly consistent with the primary winds (see Figs. 1a and 1b of *Fenton and Richardson* [2001b]). Summer evening winds come from the ENE following the diurnal tide, and summer afternoon winds come from the WSW following a deflection of Hadley circulation winds (see Plates 1c and 1d of *Fenton and Richardson* [2001b]). The daytime wind that *Fenton and Richardson* [2001b] found matched bright streaks is responsible for creating dust devil tracks, and the evening wind that they found matched dark streaks is the tertiary wind that also produces one of the dune slipface directions. Modeled winds aligned with the secondary winds are absent from the GFDL Mars GCM runs as well as the Mars MM5 runs described here. Therefore, the Mars MM5 runs are consistent with

global model results, and no large-scale effects have been erased by the use of a small domain.

Further possible sources of the secondary winds must be considered. For example, there may be unusual but strong storms that occasionally pass through the area, with wind gusts that carry large quantities of sand. Such storms may be infrequent enough that they are not predicted by GCM's, but of enough strength that the secondary slipfaces are maintained.

If the secondary winds are instead produced by a common annually-reproduced wind pattern, then a method must be found for discovering why they are not represented in this work. A number of craters in Noachis Terra contain dunefields, each of which has slipfaces indicating the strongest surface winds that influence the area. If these secondary winds persist throughout the region, perhaps to different degrees in different dunefields, then an understanding of the regional distribution of winds can be gained. A potential way to resolve the issue of the missing wind is to model winds over nearby craters to determine if these secondary winds are predicted elsewhere, and how well those predictions match the dune morphology.

Regardless of the missing secondary wind, the Mars MM5 successfully predicts all other wind orientations indicated by aeolian features on the surface. The primary winds are fall and winter afternoon westerlies that dominate the crater floor. The tertiary winds are spring and summer evening easterly katabatic flows that are concentrated in the eastern portion of the crater floor, consistent with observed dune slipfaces. These tertiary winds also explain the trapping of sand in crater floors, for they oppose the primary winds that move sand through the area. The tertiary winds are present throughout the region but they are only strong enough on the crater floors to counter the strong primary winds. Dust devil tracks are

produced by weak early afternoon westerly spring and summer winds produced by planetary rotation. The Mars MM5 results explain the source of the winds that produce aeolian features, making it a useful tool for understanding and predicting aeolian processes on the Martian surface.

## 5. Acknowledgements